Desalination and Water Treatment
www.deswater.com

doi: 10.5004/dwt.2022.28438

262 (2022) 168–179
June

Effective removal of Cd(II) from aqueous solution by $MnFe_2O_4$ composite modified by surfactant

Xuan Cao, Hui Liu, Bo Wang, Cheng Zhang, Shuhua Yao*

Shenyang University of Chemical Technology, Shenyang 110142, China, emails: ysh1997@163.com (S. Yao), caoxuan@syuct.edu.cn (X. Cao), liuhui999oo@163.com (H. Liu), Wb18740162083@163.com (B. Wang), 13604066900@163.com (C. Zhang)

Received 29 December 2021; Accepted 27 March 2022

ABSTRACT

In this study, the CTAB/$MnFe_2O_4$/MnO_2 and $MnFe_2O_4$/MnO_2 composites were prepared using the co-precipitation method. Fourier-transform infrared spectroscopy, scanning electron microscopy, X-ray diffraction, and Brunauer–Emmett–Teller method were employed to characterize their morphology and structure. Furthermore, the selective adsorption properties of Cd(II) were investigated under different conditions. The findings support the hypothesis that the optimal adsorption pH for Cd(II) is 6. The adsorption process as a whole fits well the pseudo-second-order kinetic model, and the intraparticle diffusion model is not the only rate-controlling step that is greatly influenced by the film diffusion process. The Langmuir isotherm model of monolayer adsorption behavior describes well the removal of Cd(II) *via* adsorption onto the $MnFe_2O_4$ composites. According to the Dubinin–Radushkevich model, the adsorption of Cd(II) by CTAB/$MnFe_2O_4$/MnO_2 is chemisorption in nature. The effects of competing ions on Cd(II) adsorption using CTAB/$MnFe_2O_4$/MnO_2 are as follows: Ca(II) > Mg(II) > Na(I). The promoting effect of organic acids on Cd(II) follows the order of citric acid > tartaric acid > oxalic acid. As a result, the modified $MnFe_2O_4$ composite is a potential adsorbent for Cd(II) ion removal from aqueous solutions.

Keywords: Adsorbent; Cd(II); Composite; $MnFe_2O_4$; Surfactant

1. Introduction

Cadmium can enter the water through electroplating, discharge from metal smelters, alloy preparation, waste battery treatment, and cadmium-plated steel scrap recycling [1]. Cadmium has been identified as one of the most dangerous heavy metals [2]. Because it is non-biodegradable and easily enriched in organisms, it can cause kidney damage, bone degeneration, hypertension, emphysema, nervous system damage, and even cancer [3,4]. Therefore, it is very crucial to remove Cd(II) from aqueous solution efficiently and economically.

To date, several methods for cadmium removal have been developed, including chemical precipitation, ion exchange, electrochemical methods, and adsorption. Among them, adsorption is the most advantageous method for water treatment owing to its high efficiency, ease of operation, and low-cost [5,6]. Therefore, many adsorbents have been developed to remove Cd(II) from wastewater [7]. Carbon nanotubes can effectively remove Cd(II), but the price is expensive, while activated carbon has an obvious effect of removing Cd(II), but it is easy to desorption [8,9]. Compared with traditional adsorption materials, $MnFe_2O_4$ has attracted considerable attention owing to its high magnetic properties, easy separation, strong stability, and large specific surface area. It has also been reported that $MnFe_2O_4$ has a significant effect on heavy metal removal from aqueous solutions. $MnFe_2O_4$ in combination with ferrous ions removes Cr(VI), $MnFe_2O_4$ in combination with graphene oxide removes lead and arsenic, and $MnFe_2O_4$ in

* Corresponding author.

combination with biochar removes Tl [10–12]. Therefore, we speculate that these $MnFe_2O_4$ composites may have a certain effect on Cd(II) removal.

According to some studies, modification of $MnFe_2O_4$ can improve the removal ability of some difficult-to-separate metal ions [13]. MnO_2 is an efficient and cost-effective adsorbent that has a positive effect on heavy metal adsorption in wastewater. Because the Fe_3O_4-MnO_2 composite material has been used to remove heavy metals from water [14], a MnO_2-modified $MnFe_2O_4$ composite material can be prepared to improve the adsorption capacity of adsorbents. In recent years, an increasing attention has been paid to the study of selective adsorbents. It is a good way to improve the selectivity of adsorbents *via* surface modification. Cetyltrimethylammonium bromide (CTAB) is a widely used as cationic surfactant [15]. Because of the hydrophobic groups on its surface, which can change the surface properties and surface charges of the substance, thereby improving the adsorption capacity of the adsorbent. As a result, CTAB was selected to further modify the $MnFe_2O_4$/MnO_2 composite material to synthesize CTAB/$MnFe_2O_4$/MnO_2 in order to improve adsorbent selectivity.

To date, materials like CTAB/$MnFe_2O_4$/MnO_2 and their selective performance in adsorbing Cd(II) from mixtures have never been reported. Thus, it is necessary to investigate the adsorption of Cd(II) by the CTAB/$MnFe_2O_4$/MnO_2 composite. In this study, the co-precipitation method was employed to develop CTAB/$MnFe_2O_4$/MnO_2 and $MnFe_2O_4$/MnO_2 magnetic composites. The adsorbents that were created were characterized, and their adsorption properties for Cd(II) were compared under various experimental conditions. Then, some parameters such as the effects of pH, contact time, temperature, initial concentration, interference of coexisting ions, and coexistence of organic acids on the adsorption efficiency were studied.

2. Materials and methods

2.1. Materials

All the chemical reagents used in this study were of analytical grade and did not require further purification. They were purchased from Sinopharm Chemical Reagents Co., Ltd., (Shanghai, China). Drugs include $FeCl_3·6H_2O$, $MnCl_2·4H_2O$, $FeSO_4·7H_2O$, NaOH, $MnSO_4$, $KMnO_4$, cetyltrimethylammonium bromide (CTAB > 99.0%), and the water used to prepare various solutions in the experiment is deionized water. All the adsorption experiments were replicated thrice, and the mean values thus obtained were considered as the final results.

2.2. Preparation of $MnFe_2O_4$/MnO_2 and CTAB/$MnFe_2O_4$/MnO_2 composites

$MnFe_2O_4$/MnO_2 and CTAB/$MnFe_2O_4$/MnO_2 can be prepared according to the procedure described in Fig. 1.

2.2.1. Synthesis of $MnFe_2O_4$ and CTAB/$MnFe_2O_4$

$MnFe_2O_4$ can perform a synthesis similar to those in previous reports [16]. After dispersing 0.056 mol of $FeCl_3·6H_2O$ in 200 mL deionized water and heating it to 60°C in the water bath, $MnCl_2·4H_2O$ (0.024 mol) and $FeSO_4·7H_2O$ (0.024 mol) were added to the mixed solution to achieve a Mn(II)/Fe molar ratio of 0.3. Then, under constant agitation, the NaOH (1 M, heated to the same temperature) solution was added dropwise to the mixed solution for co-precipitation reaction until the pH was kept at about 11. After 3 h, the mixture was separated after aging at 60°C for 1 h and washed with deionized water three to five times until the pH of the filtrate was around 7. Finally, it was vacuum-dried for 24 h at 60°C. The synthesis of CTAB/$MnFe_2O_4$ is similar to that of $MnFe_2O_4$ [17], except that 0.2 g of CTAB was added before the addition of NaOH; the other steps are also the same.

2.2.2. Synthesis of $MnFe_2O_4$/MnO_2 and CTAB/$MnFe_2O_4$/MnO_2

According to previous methods, MnO_2 was introduced into the surface of $MnFe_2O_4$ and CTAB/$MnFe_2O_4$ [18], 2 g $MnFe_2O_4$ or CTAB/$MnFe_2O_4$ was dissolved in 100 mL deionized water. The solution was ultrasonically treated for 10 min at room temperature (0.4 g CTAB was added to the CTAB/$MnFe_2O_4$ solution), then heated to 60°C and stirred continuously for 30 min. $MnSO_4$ (0.036 M, 240 mL) and

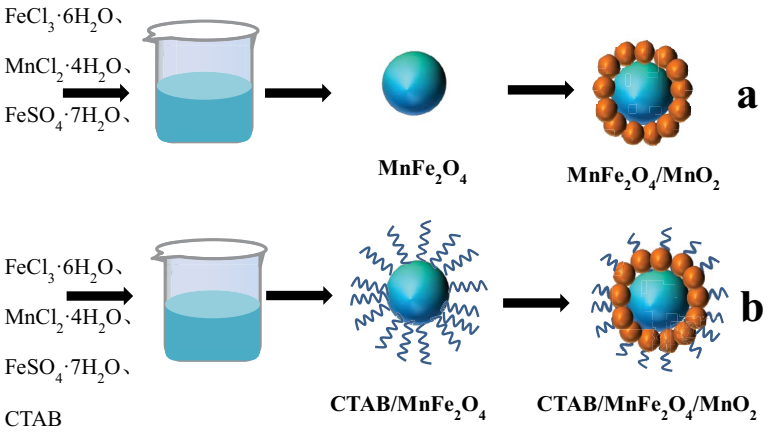

Fig. 1. Synthesis route of $MnFe_2O_4$/MnO_2 (a) and CTAB/$MnFe_2O_4$/MnO_2 (b).

$KMnO_4$ (0.036 M, 160 mL) were slowly added to the solution, and the resulting mixture was heated in a water bath at 60°C for 4 h and stirred continuously. Under the same conditions, the mixture was aged for 1 h. After washing and drying, $MnFe_2O_4/MnO_2$ and CTAB/$MnFe_2O_4/MnO_2$ composites were prepared for subsequent experiments.

2.3 Characterization

The morphology of the adsorbents was analyzed by scanning electron microscopy (JMS-6360LV, JEOL, Japan). The adsorbents were mounted on pin stubs by use of double-sided carbon tape and sputter-coated with gold, and imaged at 30 kV. Information of crystal structure was obtained from X-ray diffraction spectra (X'Pert PRO MPD, PANalytical, Netherlands). A scanning rate of 0.02°/s was applied to record the patterns in the 2θ angle range from 10° to 90°. Data of specific surface area was calculated by the methods of Brunauer–Emmett–Teller (BET) (SSA-6000, Beijing Builder, China). Fourier-transform infrared (FTIR) spectra were obtained from the (Thermo Nicolet Corp, Madison, WI, USA)spectrometer. The KBr/sample discs were prepared by mixing 0.5% of finely ground samples in KBr. The samples were scanned in FTIR range (400–4,000 cm^{-1}) with the resolution of 4 cm^{-1}.

2.4. Adsorption experiments

2.4.1. Effect of pH on adsorption

Experiments were conducted to determine the effect of pH on adsorption by adding 0.1 g of adsorbent and 100 mL of 3 mg L^{-1} Cd(II) solution into a series of conical flasks and adjusting the pH of the solution to 3.0–10.0 [19]. The concentration selected is based on the concentration of Cd(II) in the actual wastewater [20]. Then, it was shaken in a shaker at 25°C for 24 h. The removal rate was calculated using Eq. (1):

$$U\% = \left[\frac{\left(C_0 - C_t\right)}{C_0}\right] \times 100 \tag{1}$$

where C_0 (mg L^{-1}) denotes the initial concentration of metal ions, and C_t (mg L^{-1}) is the concentration of metal ions after adsorption.

2.4.2. Adsorption kinetic

The batch method was employed for the kinetic experiments. In 500 mL of 3 mg L^{-1} Cd(II) solution, 0.5 g of the $MnFe_2O_4/MnO_2$ or CTAB/$MnFe_2O_4/MnO_2$ adsorbent was added, and the pH was adjusted with 0.1 M HNO_3 and NaOH. The mixture was oscillated on a shaker at 160 rpm for 24 h, taking samples at different intervals. The same amount of samples was filtered and stored with a 0.22 μm filter membrane for subsequent measurement. The remaining concentration of Cd(II) in the solution was measured using the atomic absorption spectrophotometer (AAS) at various time intervals. The following equation can be used to calculate the number of pollutants adsorbed per unit mass of adsorbent in each time interval Eq. (2):

$$q_t = \frac{\left(C_0 - C_t\right)V}{W} \tag{2}$$

where q_t (mg g^{-1}) denotes the adsorption capacity at time t; C_0 and C_t, the initial and concentration of Cd(II) in solution at time t, respectively; V (mL), the volume of solution; and W (g), the mass of adsorbent.

The kinetic study can obtain information on the adsorption mechanism. The pseudo-first-order kinetic model, pseudo-second-order kinetic model, and intraparticle diffusion model were used to simulate the experimental data to determine the appropriate adsorption kinetic model. Their linear equations are expressed as follows [21–24]:

$$\ln\left(q_e - q_t\right) = \ln q_e - K_1 t \tag{3}$$

$$\frac{t}{q_t} = \frac{1}{K_2 q_e^2} + \frac{t}{q_e} \tag{4}$$

$$q_t = K_{ip} t^{1/2} + C \tag{5}$$

where q_e and q_t denote the adsorption capacity at equilibrium and time t, respectively (mg g^{-1}). K_1, K_2, and K_{ip} are the rate constants for the pseudo-first-order kinetic, pseudo-second-order kinetic, and intraparticle diffusion models (min^{-1}, mg g^{-1} min, mg g^{-1} $min^{-0.5}$), respectively. t denotes the adsorption time (min) and C the experimental constant of boundary layer thickness.

2.4.3. Isothermal adsorption

At pH = 6.0, isothermal adsorption was performed by mixing 0.1 g of adsorbent with 100 mL of Cd(II) solution with initial concentration of 3, 50, 70, 100, 150, 200, 300, and 400 mg L^{-1}. For 24 h, the mixture was shaken at various temperatures. Subsequently, the concentration of the residual metal ions was determined, and the adsorption capacity was calculated.

3. Results and discussion

3.1. Characterization of $MnFe_2O_4/MnO_2$ and CTAB/$MnFe_2O_4/MnO_2$

X-ray diffraction (XRD) can be used to determine the crystal structure of the material. Fig. 2 presents the XRD patterns of $MnFe_2O_4$, $MnFe_2O_4/MnO_2$, and CTAB/$MnFe_2O_4/MnO_2$. The XRD of $MnFe_2O_4$ reveals a strong diffraction peak when the values of 2θ are 18.0°, 29.7°, 34.9°, 36.5°, 42.4°, 52.6°, 56.1°, 61.6°, and 72.8°, which are attributed to the planes (111), (220), (311), (222), (400), (422), (333), (440), and (533). The results were also consistent with the standard card (JCPDS: 74-2403) [25,26]. In general, the XRD peaks do not significantly change after the introduction of MnO_2 and CTAB, indicating that such an introduction

does not affect the crystal structure of $MnFe_2O_4$, which is consistent with the results of relevant literature [27]. However, the peak strength of the b and c composites was weaker than that of a composite, which could be attributed to MnO_2 and CTAB weakening the diffraction peak intensity of $MnFe_2O_4$.

The scanning electron microscopy (SEM) images of $MnFe_2O_4/MnO_2$ and CTAB/$MnFe_2O_4/MnO_2$ are presented in Fig. 3. As can be seen from Fig. 3a, the $MnFe_2O_4/MnO_2$ composite is spherical, which is consistent with the shape of $MnFe_2O_4$ [28,29]. Spherical molecules have a layer of small aggregates on the surface, and the molecules are tightly stacked with small spaces. The small particle filling of these spaces may result in a decrease in specific surface area. After combining $MnFe_2O_4/MnO_2$ with CTAB, many netlike structures form around the sphere, as presented in Fig. 3b, increasing the distance between single spherical molecules. Compared with $MnFe_2O_4/MnO_2$, this network structure may be the CTAB.

The specific surface areas of $MnFe_2O_4/MnO_2$ and CTAB/$MnFe_2O_4/MnO_2$ were found to be 132.947 and 166.574 $m^2\ g^{-1}$, respectively, using the BET method. The results indicate that after loading CTAB, the specific surface area increases [30], which is consistent with the SEM analysis results, and this increase is expected to improve metal ion adsorption. Most importantly, we found that after the reaction with metal ions, their specific surface area decreased to 50.745 and 78.653 $m^2\ g^{-1}$ respectively, mainly because metal ions were adsorbed to the surface of the composite material.

The FTIR spectra of $MnFe_2O_4/MnO_2$ and CTAB/$MnFe_2O_4/MnO_2$ are presented in Fig. 4. In the spectrum of $MnFe_2O_4/MnO_2$ and CTAB/$MnFe_2O_4/MnO_2$, O–H exhibited the characteristic vibration absorption peak at 3,419 cm^{-1}. The stretching vibration of Fe–O is responsible for the characteristic vibration absorption peaks at 566 cm^{-1} [31,32]. The absorption peak of O–H was significantly increased after loading CTAB, indicating that CTAB was introduced. For CTAB/$MnFe_2O_4/MnO_2$, the new absorption peak that appeared at 2,921 and 2,852 cm^{-1} belongs to the asymmetric and symmetric absorptions of the $–CH_2$ band [33,34], and the characteristic peak of $–CH_3$ at 1,349 cm^{-1} [35]. New characteristic peaks appeared at 1,596 and 1,114 cm^{-1}, which are attributed to the N–H and C–H stretching vibrations,

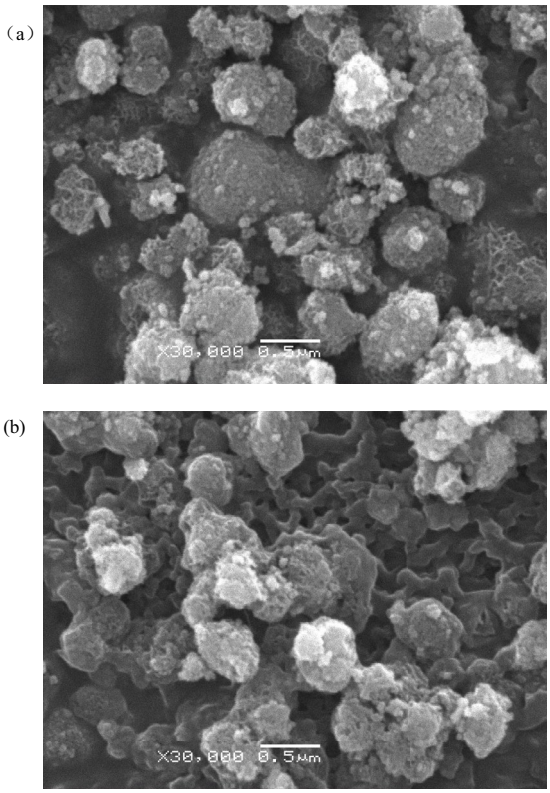

Fig. 3. SEM image of $MnFe_2O_4/MnO_2$ (a) and CTAB/$MnFe_2O_4/MnO_2$ (b).

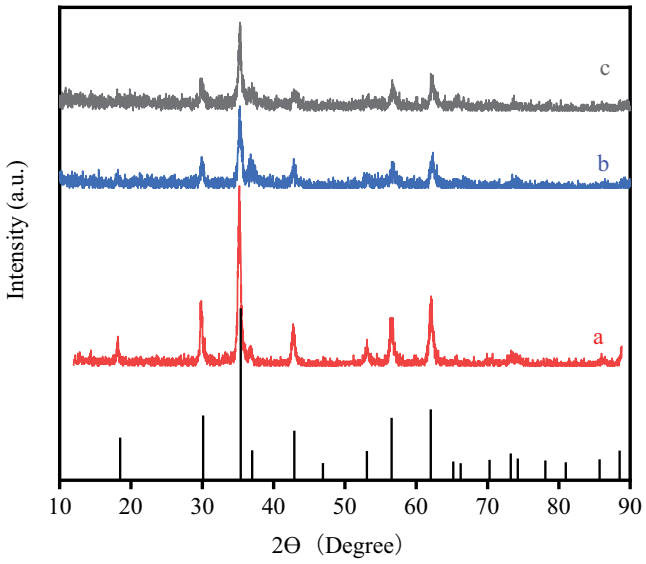

Fig. 2. XRD patterns of $MnFe_2O_4$ (a), $MnFe_2O_4/MnO_2$ (b), and CTAB/$MnFe_2O_4/MnO_2$ (c).

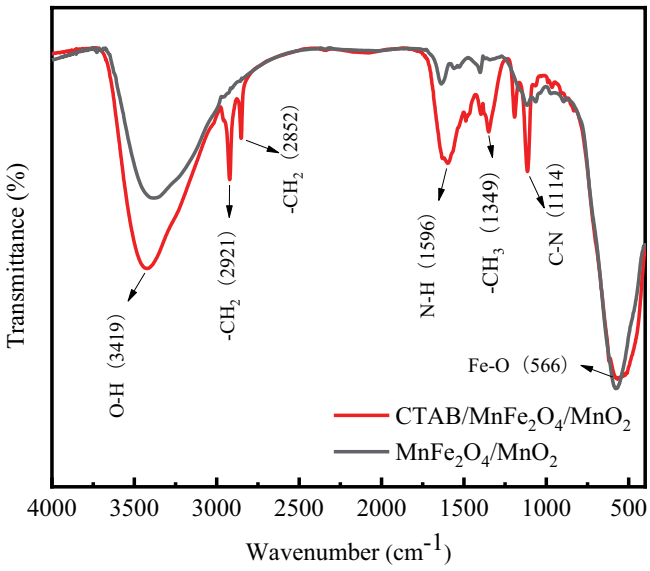

Fig. 4. FTIR spectrum of $MnFe_2O_4/MnO_2$ and CTAB/$MnFe_2O_4/MnO_2$.

respectively. A few peaks shifted after loading CTAB, which mainly involved in the interactions between the functional groups of $MnFe_2O_4/MnO_2$ composites and CTAB [36]. In conclusion, CTAB was successfully deposited on the surface of the $MnFe_2O_4/MnO_2$ composites.

3.2. Effects of pH on Cd(II) adsorption

Due to the electrostatic attraction between the adsorbent and metal ions, the pH value significantly influences the performance of the adsorbent [37]. Fig. 5 presents the influence of pH value on Cd(II) removal by $MnFe_2O_4/MnO_2$ and CTAB/$MnFe_2O_4/MnO_2$. When the pH value increases from 3 to 6, the removal rate of Cd(II) adsorbed by CTAB/$MnFe_2O_4/MnO_2$ gradually decreases from 63% to 60%. When the pH value increases from 7 to 9, the removal efficiency of Cd(II) remains nearly constant. This balance can be attributed to two reasons. First, the increase in pH value leads to an increase in negative charge and the deprotonation effect, which enhances the electrostatic attraction between the adsorbent and Cd(II). Second, lone pair electrons provided by nitrogen atoms in CTAB are bound, which reduces the ability of N atoms to form stable complexes with metal ions. When the pH is 3–4, the removal rate of $MnFe_2O_4/MnO_2$ adsorption Cd(II) begins to increase and tends to be flat when the pH is 4–9. Because the solution is too acidic, desorption of adsorbent may occur, and the solution may become too alkaline, which may easily hydrolyze with Cd(II) and cause hydroxide precipitation [38]. It is not appropriate to select a reaction system that is either too acidic or too alkaline. When the pH is set to 6, it is more in line with the acid-base environment of natural water. As a result, 6 was selected as the optimal adsorption pH value for this study.

3.3. Adsorption kinetics

Fig. 6 presents the effects of contact time on Cd(II) adsorption by CTAB/$MnFe_2O_4/MnO_2$ and $MnFe_2O_4/MnO_2$. As can be seen from the figure, the q_t of CTAB/$MnFe_2O_4/MnO_2$ is always higher than that of $MnFe_2O_4/MnO_2$ as CTAB is loaded on CTAB/$MnFe_2O_4/MnO_2$, and the surface functional groups of CTAB are abundant and selective. It can also be seen that the reaction is fast in the early stages of adsorption, and the amount of adsorption increases with time. The adsorption rate then gradually decreases, and $MnFe_2O_4/MnO_2$ and CTAB/$MnFe_2O_4/MnO_2$ reach adsorption equilibrium at approximately 270 and 400 min, respectively. The rapid adsorption rate at the initial stage of adsorption is mainly attributed to the high concentration of metal ions in the solution, which can easily diffuse to the surface of the adsorbent, and there are many binding adsorption sites on the surface of the adsorbent at the initial stage of adsorption. The adsorption rate decreases as adsorption progresses due to the accumulation of Cd(II) on the adsorbent's surface, which results in a reduction in the binding sites. Meanwhile, the concentration gradient of metal ions in the solution decreases, making it difficult for metal ions to diffuse to the surface of the adsorbent until adsorption equilibrium is reached.

The fitting results of the three dynamic models are presented in Fig. 7, and the fitting parameters are listed in Tables 1 and 2. The correlation coefficients (R^2) of the pseudo-second-order kinetic model are all greater than those of the pseudo-first-order kinetic model and the R^2 of the pseudo-second-order kinetic model is greater than 0.8 [39], and the q_e of the pseudo-second-order kinetic model is closer to the adsorption amount when the experiment reaches equilibrium, indicating that the pseudo-second-order kinetic model can accurately describe the entire adsorption process. Table 2 presents the fitting results of the intraparticle diffusion kinetic model for Cd(II) adsorption by CTAB/$MnFe_2O_4/MnO_2$ and $MnFe_2O_4/MnO_2$. This implies that the adsorption process is divided into three stages. The first stage is the diffusion of a liquid film; the second-stage, the slow gap diffusion from the adsorbent's surface to the interior of the adsorbent [40], and the third stage, the adsorption

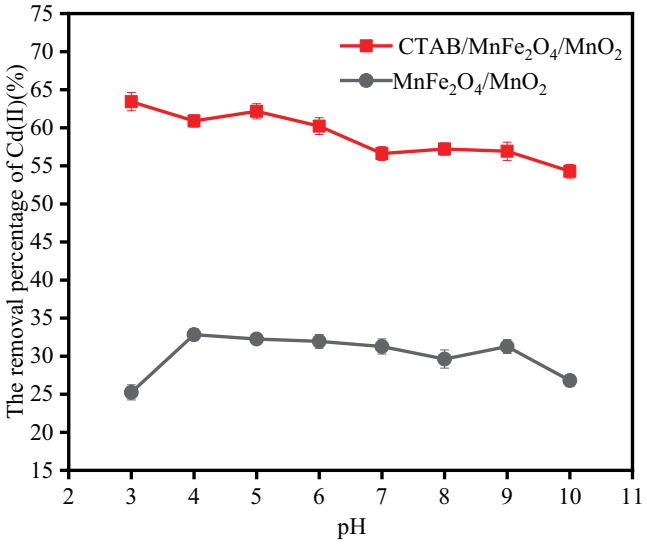

Fig. 5. Effect of pH on the adsorption of Cd(II), pH range 2–11, C_0 = 3 mg L^{-1}, dosage of adsorbent = 1 g L^{-1}, reaction time = 1,440 min, T = 298.15 K.

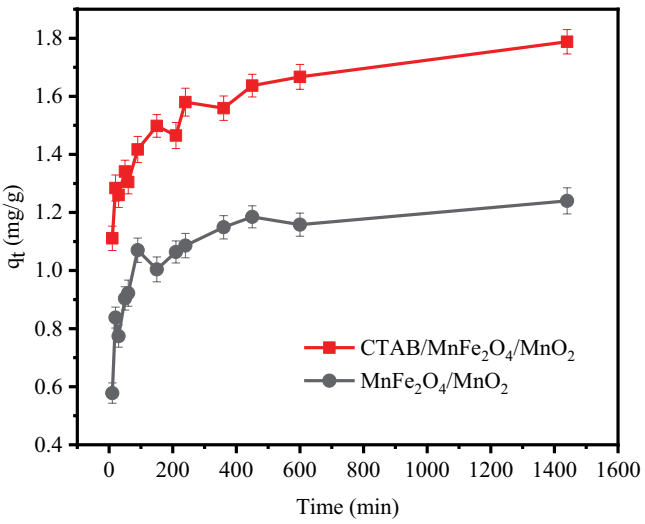

Fig. 6. Adsorption kinetic curves of CTAB/$MnFe_2O_4/MnO_2$ and $MnFe_2O_4/MnO_2$ for Cd(II) (pH = 6, C_0 = 3 mg L^{-1}, dosage of adsorbent = 1 g L^{-1}, reaction time = 1,440 min, T = 298.15 K).

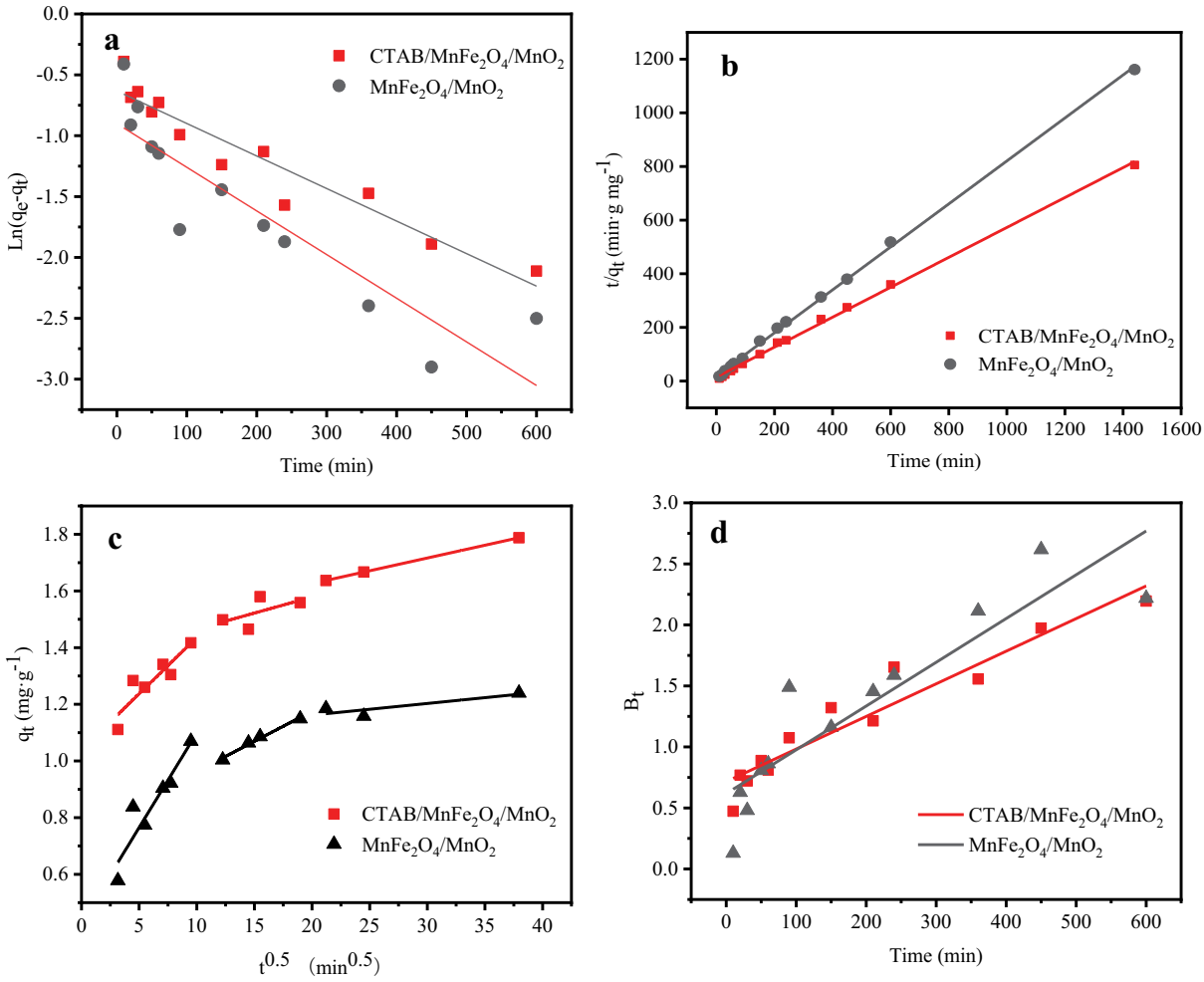

Fig. 7. Pseudo-first-order kinetic model (a) and pseudo-second-order kinetic model (b) and intraparticle diffusion model (c) and $B_t - t$ (d) for Cd(II) on CTAB/$MnFe_2O_4$/MnO_2 and $MnFe_2O_4$/MnO_2.

Table 1
Kinetic parameters for the adsorption of Cd(II)

Adsorbents	Experimental q_e (mg g^{-1})	First-order			Second-order		
		plot: $\ln(q_e - q_t)$ vs. t q_e = exp(intercept) K_1 = slope			plot: t/q_t vs. t q_e = 1/slope K_2 = slope²/intercept		
		R^2	q_e (mg g^{-1})	K_1 (1 min^{-1})	R^2	q_e (mg g^{-1})	K_2 (g mg^{-1} min^{-1})
CTAB/$MnFe_2O_4$/MnO_2	1.788	0.4190	1.51	0.1068	0.9981	1.79	0.0210
$MnFe_2O_4$/MnO_2	1.24	0.7307	1.09	0.0558	0.9991	1.24	0.0331

equilibrium. The *C* value is not zero, and these curves do not pass through the origin, which means that the adsorption mechanism of Cd(II) on CTAB/$MnFe_2O_4$/MnO_2 and $MnFe_2O_4$/MnO_2 is complex, and the intraparticle diffusion is not the only rate-limiting step.

To determine whether the rate-controlling step is an intraparticle diffusion process or a film diffusion process, the following Boyd film diffusion model equation is used [41]:

$$F = 1 - \left(\frac{6}{\pi^2}\right)\sum_{n=1}^{\infty}\left(\frac{1}{n^2}\right)\exp\left(-n^2 B_t\right) \quad (6)$$

where B_t is a constant of time; n, an integer that defines infinite series solutions; and F, the ratio of adsorption capacity at t to adsorption capacity at equilibrium: $F = q_t/q_e$. Eq. (7) can be obtained by substituting the F value for the Boyd model.

$$B_t = -0.498 - \ln\left(1 - \frac{q_t}{q_e}\right) \quad (7)$$

The B_t values at different times can be obtained from Eq. (7). The rate-controlling steps of the reaction can be determined using a fitting diagram of B_t to time t, as presented in Fig. 8. The fitting curve is close to the origin at the beginning of the reaction, indicating that the reaction is more prone to intraparticle diffusion [42]. As the reaction progresses, the curve slope increases, and the $MnFe_2O_4/MnO_2$ fitting curve intercept is larger than the CTAB/$MnFe_2O_4/MnO_2$ fitting curve. Neither curve passes through the origin, indicating that film diffusion is the main rate-controlling step.

3.4. Adsorption isotherm

Adsorption isotherms are essential for understanding adsorbent properties and providing information on how adsorbents interact with adsorbents [43]. Fig. 9 presents the isothermal adsorption curves of CTAB/$MnFe_2O_4/MnO_2$ and $MnFe_2O_4/MnO_2$ for Cd(II). The results indicate that the adsorption capacity increases with the increase in Cd(II) ion concentration, and the adsorption capacity of CTAB/$MnFe_2O_4/MnO_2$ is higher than that of $MnFe_2O_4/MnO_2$, which indicates that CTAB/$MnFe_2O_4/MnO_2$ has a better selectivity for Cd(II); this finding is consistent with the results of adsorption kinetics. The adsorption capacity increases as the temperature increases, indicating that the adsorption process is endothermic.

The adsorption equilibrium data were studied using theoretical or empirical equations. In this study, the Langmuir and Freundlich models were used to analyze the experimental data of isothermal adsorption. The Langmuir model describes the noninteractive homogeneous monolayer adsorption of molecules on solid surfaces, whereas the Freundlich model is an empirical equation. The equations of the two models are as follows:

Table 2
Intraparticle diffusion parameters for the adsorption of Cd(II)

Adsorbent	Ion	CTAB/$MnFe_2O_4$/MnO_2	$MnFe_2O_4$/MnO_2
K_{ip1} (mg g^{-1} $min^{-0.5}$)		0.0398	0.0668
C_1		1.0384	0.4311
R^2		0.8144	0.8744
K_{ip2} (mg g^{-1} $min^{-0.5}$)		0.0113	0.0213
C_2	Cd(II)	1.3519	0.7503
R^2		0.3549	0.9871
K_{ip3} (mg g^{-1} $min^{-0.5}$)		0.009	0.0041
C_3		1.4461	1.0800
R^2		0.9999	0.7575

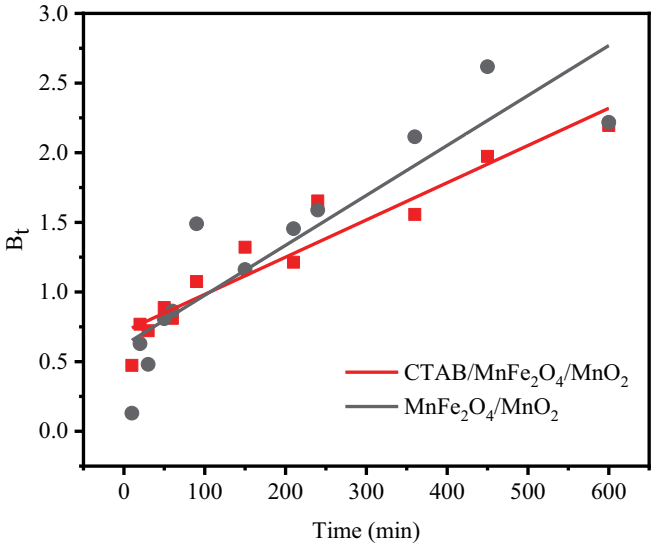

Fig. 8. Fitting figure of B_t values t.

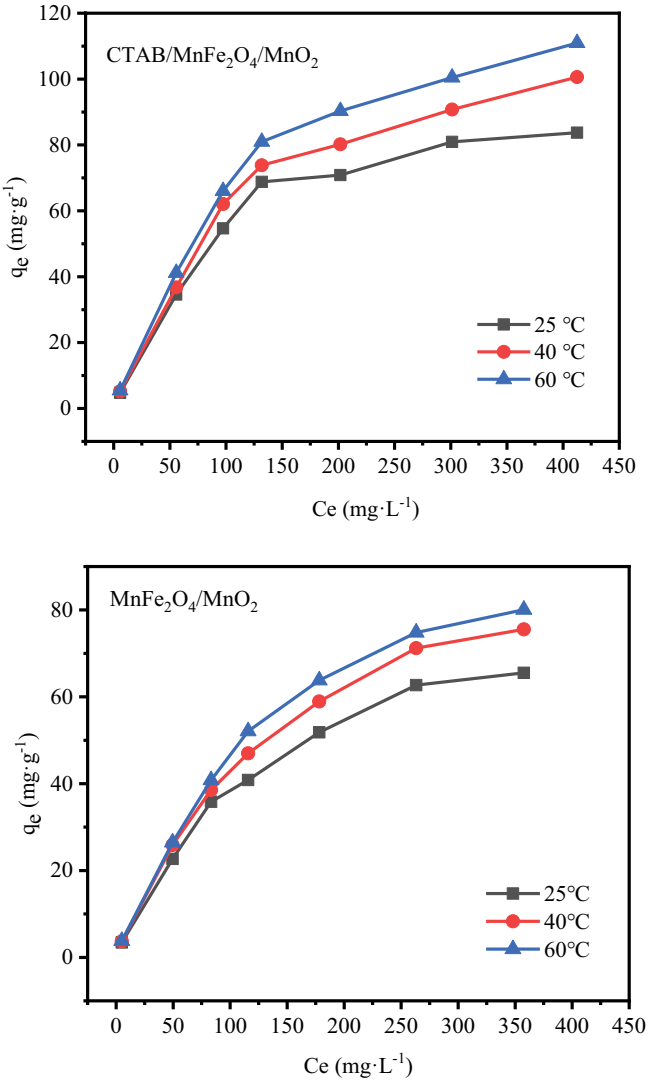

Fig. 9. Isotherm adsorption curves of CTAB/$MnFe_2O_4/MnO_2$ and $MnFe_2O_4/MnO_2$ for Cd(II).

Langmuir model: $$\frac{C_e}{q_e}=\frac{C_e}{q_m}+\frac{1}{q_m K_L} \quad (8)$$

Freundlich model: $$\ln q_e=\ln K_F+\frac{\ln C_e}{n} \quad (9)$$

where C_e (mg L^{-1}) and q_e (mg g^{-1}) are the metal ion concentration and adsorption capacity at equilibrium, respectively; q_m (mg g^{-1}), the maximum adsorption capacity of monolayer adsorption; K_L and K_F, the Langmuir and Freundlich constants, respectively; and n(dimensionless), the adsorption strength index. A value of 1–10 indicates that the reaction is progressing [44]. Their values can be calculated using the intercepts and slopes of the linear plots C_e/q_e vs. C_e and $\ln q_e$ vs. $\ln C_e$, respectively.

The fitting parameters of the Langmuir and Freundlich models are presented in Table 3. It can be seen that the correlation coefficient of the Langmuir model (R^2) was higher than that of the Freundlich model (R^2), indicating that the uptake of Cd(II) can be well described by the Langmuir model with monolayer adsorption behavior. Furthermore, the q_m calculated using the Langmuir model fitting for the Cd(II) adsorption of CTAB/$MnFe_2O_4$/MnO_2 at various temperatures is greater than that of $MnFe_2O_4$/MnO_2, which is completely consistent with previous research. The n values in Table 3 are all in ($1 < n < 10$), indicating that both absorbents are beneficial to the adsorption process. Table 4 presents a comparison of q_m with other alternative adsorbents. Because CTAB/$MnFe_2O_4$/MnO_2 has a higher adsorption capacity than other adsorbents, it is expected to be used in the removal of Cd(II) from an aqueous solution as well as in the modern process of extraction and concentration of metal cadmium.

Another highly regarded adsorption isotherm model is the Dubinin–Radushkevich model, which is used to determine whether the adsorption reaction is physical or chemical [52,53]. The linear equation of the Dubinin–Radushkevich isotherm can be expressed as follows:

$$\ln q_e=\ln q_m-\beta\varepsilon^2 \quad (10)$$

$$\varepsilon=RT\ln\left(1+\frac{1}{C_e}\right) \quad (11)$$

where ε (kJ^2 mol^{-2}) is Polanyi potential, and β (mol^2 J^{-2}) is the activity coefficient related to the mean free energy (E, kJ mol^{-1}) of the adsorption. The mean free energy E (kJ mol^{-1}) is calculated from as follows:

$$E=\frac{1}{\sqrt{2\beta}} \quad (12)$$

Table 3
Parameters of adsorption isotherm models for CTAB/$MnFe_2O_4$/MnO_2 and $MnFe_2O_4$/MnO_2

Adsorbent	Ion	T (°C)	Langmuir			Freundlich		
			q_m (mg g^{-1})	K_L (L mg^{-1})	R^2	K_F (mg g^{-1})(L $mg^{-1/n}$)	n	R^2
CTAB/$MnFe_2O_4$/MnO_2	Cd(II)	25	89.85	0.0387	0.9969	6.2216	1.98	0.9359
		40	105.6	0.0375	0.9907	9.6100	2.11	0.9557
		60	115.21	0.0474	0.9930	11.5662	2.29	0.9662
$MnFe_2O_4$/MnO_2		25	77.28	0.0184	0.9877	3.0680	1.73	0.9777
		40	88.18	0.0196	0.9885	3.6705	1.74	0.9797
		60	92.94	0.0210	0.9910	3.9278	1.73	0.9764

Table 4
Comparison of the maximum adsorption capacities for Cd(II) onto different adsorbents in this work with other adsorbents reported in earlier studies.

Adsorbents	q_m (mg g^{-1})	pH	References
Bis(2,4,4-trimethylpentyl) phosphoric acid magnetite–manganese oxide xerogel (mMOX)	7.79	6	[45]
MCCR-550	29.8	5.5	[46]
$CaCO_3$-modified biochar	36.5	6	[47]
MnO_2-biochar	45.8	5 ± 0.2	[48]
Mushroom substrate biochars	46.87	4–7	[49]
Magadiite impregnated with	49.45	2	[50]
Fe_3O_4@SiO_2-HE-S	56	6	[51]
Solid-phase magadiite	64.06	2	[50]
$MnFe_2O_4$/MnO_2	77.28	6	This study
CTAB/$MnFe_2O_4$/MnO_2	89.85	6	This study

If E < 8 kJ mol^{-1}, the adsorption is physical, and the E value between 8, and 16 kJ mol^{-1} indicates that the adsorption process is chemical. Table 5 presents the fitting parameters of the Dubinin–Radushkevich model. The E values of CTAB/$MnFe_2O_4$/MnO_2 at various temperatures are all between 8 and 16 kJ mol^{-1}, indicating that the adsorption of CTAB/$MnFe_2O_4$/MnO_2 for Cd(II) is chemical.

3.5. Adsorption thermodynamics

The spontaneity of adsorption can be explained by thermodynamic parameters. The thermodynamic parameters of ΔG (kJ mol^{-1}), ΔH (kJ mol^{-1}) and ΔS (J mol^{-1} K^{-1}) were calculated using Gibbs free energy and the Van't Hoff equation, respectively. The equations are expressed as follows [54,55]:

$$\Delta G = -RT\ln K_C \tag{13}$$

$$K_C = \frac{q_e}{C_e} \tag{14}$$

$$\ln K_C = \frac{\Delta S^\circ}{R} - \frac{\Delta H}{RT} \tag{15}$$

$$K^\circ = 1{,}000 K_L \times MA \tag{16}$$

where T (K) and R (8.314 J mol^{-1} K^{-1}) are the thermodynamic temperatures and ideal gas constant, respectively; ΔG, ΔH, and ΔS are Gibbs free energy, enthalpy, and entropy changes, respectively; and K_L (L mol^{-1}) is the Langmuir constant. Table 6 presents the calculated thermodynamic parameters. The values of ΔG are all negative, indicating that the adsorption process of CTAB/$MnFe_2O_4$/MnO_2 and $MnFe_2O_4$/MnO_2 for Cd(II) was spontaneous and that the values of ΔG become more negative with increasing temperature, implying that high temperature favored adsorption [26]. The positive value of ΔH indicates that the adsorption process of Cd(II) is endothermic, and the positive value of ΔS indicates that the adsorption process is a randomness-increasing process.

3.6. Influence of coexisting ions

In general, ionic strength and the presence of anions and cations in the solution have a significant effect on the adsorption of metal ions. This is due to the coexisting ions' electrostatic attraction or repulsion with the adsorbent. Different salts (Ca(II), Mg(II), Na(I), NO_3^-, and PO_4^{3-}) were added to the Cd(II) solution to test the effects of different ions and ion strength on the adsorption capacity of adsorbents. The results are presented in Fig. 10. It can be seen that in the presence of common cations, Mg(II) and Na(I) have a slight effect on the removal of Cd(II) when the ionic strength is 0.001 M, and Mg(II) has a slightly greater inhibitory ability than Na(I). However, when the ionic strength is increased to 0.02 M, Mg(II) and Na(I) have an inhibitory effect on the removal of Cd(II). In contrast, Ca(II) has a significant influence on Cd(II) removal, especially as ionic strength increases, which is consistent with the previous report that Ca(II) has a significant influence on Cd(II) removal [56]. The order of inhibitory ability is Ca(II) > Mg(II) > Na(I); the first reason is that cations have competitive adsorption with Cd(II), and the second reason is that the Ca(II) radius is relatively large, and the polarization effect is stronger and easier to combine with CTAB, so the removal effect of Cd(II) is greater. NO_3^- has almost no effect on the removal of Cd(II) from an aqueous solution,

Table 5
Fitting parameters of Dubinin–Radushkevich model

Adsorbent	T (°C)	q_m (mg L^{-1})	B (mol^2 J^{-2})	E (kJ mol^{-1})	R^2
CTAB/$MnFe_2O_4$/MnO_2	25	76.71	–6.28 × 10^{-9}	8.923	0.9378
	40	87.36	–5.02 × 10^{-9}	9.980	0.9399
	60	94.63	–2.56 × 10^{-9}	13.975	0.8968
$MnFe_2O_4$/MnO_2	25	56.26	–1.18 × 10^{-9}	20.585	0.8703
	40	62.80	–8.24 × 10^{-9}	7.789	0.8311
	60	68.03	–7.34 × 10^{-9}	8.253	0.8775

Table 6
Thermodynamic parameters for CTAB/$MnFe_2O_4$/MnO_2 and $MnFe_2O_4$/MnO_2

Adsorbent	Ion	T (°C)	ΔG (kJ mol^{-1})	ΔH (kJ mol^{-1})	ΔS (J mol^{-1} K^{-1})
CTAB/$MnFe_2O_4$/MnO_2	Cd(II)	25	–25.24	4.96	100.90
		40	–26.42		
		60	–28.76		
$MnFe_2O_4$/MnO_2		25	–21.50	3.11	82.57
		40	–22.75		
		60	–24.39		

but its ionic strength has a significant effect on the removal of Cd(II). However, in the presence of PO_4^{3-}, the removal rate of Cd(II) approaches 100%, which could be due to the formation of an insoluble complex between PO_4^{3-} and Cd(II).

3.7. Effects of organic acids on Cd(II) adsorption

There are many organic compounds in wastewater. Organic acid is one of the many organic compounds found in wastewater. When organic acids coexist with the metal ion Cd(II), they will compete for Cd(II) adsorption. Therefore, it is necessary to further investigate the effects of mixing organic acids and metal ions on adsorbent properties. To investigate the effect of organic acids on Cd(II) adsorption, organic acids (citric acid, tartaric acid, and oxalic acid) with concentrations ranging from 0 to 100 mg L^{-1} were added to a Cd(II) (300 mg L^{-1}) solution. The results are presented in Fig. 11. When the concentration of citric acid is in the range of 0–3 mg L^{-1}, the adsorption amount of Cd(II) increases, and then gradually decreases with the increase in acid concentration; subsequently, it reaches equilibrium. The changing trend of oxalic acid is similar to that of citric acid. On the contrary, the effect of tartaric acid on Cd(II) adsorption at a concentration range of 0–3 mg L^{-1} shows that the adsorption amount increases, and then tends to reach equilibrium, with no decrease stage observed. In general, the presence of organic acids is beneficial to the removal of cadmium, and the promotion sequence is citric acid > tartaric acid > oxalic acid [57,58]. Organic acids promote Cd(II) adsorption most likely because they contain carboxyl groups, and carboxyl groups will form complexes with Cd(II); the more carboxyl groups there are, the more complexes will form.

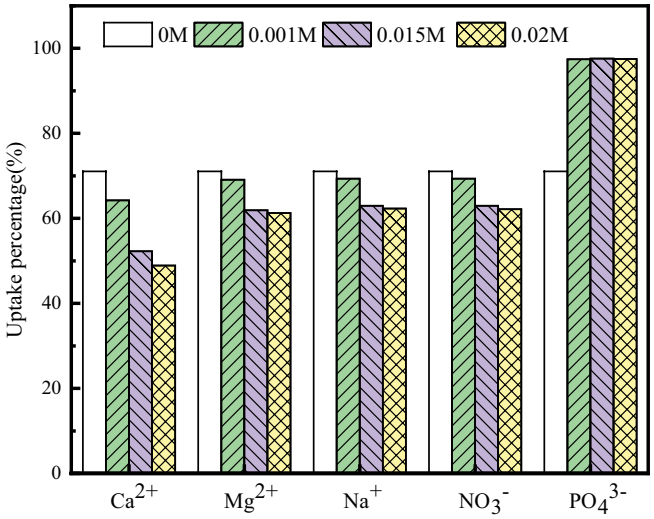

Fig. 10. Effect of coexisting ions and ionic strength on Cd(II) adsorption onto CTAB/$MnFe_2O_4$/MnO_2.

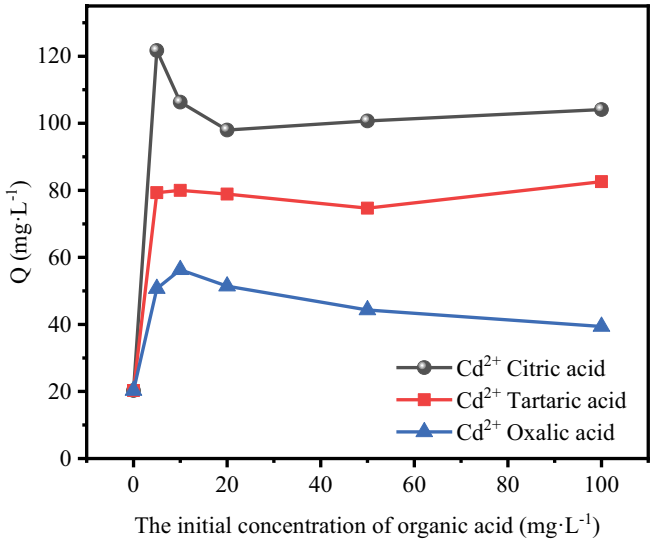

Fig. 11. Effect of organic acids on Cd(II) adsorption isotherms (pH = 6, C_0 = 300 mg L^{-1}, adsorbent dosage 1 g L^{-1}, T = 25°C, time = 1,440 min).

3.8. Adsorption mechanism

CTAB/$MnFe_2O_4$/MnO_2 and $MnFe_2O_4$/MnO_2 can remove Cd(II) mainly for the following reasons. Firstly, both CTAB/$MnFe_2O_4$/MnO_2 and $MnFe_2O_4$/MnO_2 have relatively large specific surface areas, which can effectively remove Cd(II). Secondly, CTAB/$MnFe_2O_4$/MnO_2 composite material has a large number of CTAB, and the N atoms in CTAB can provide lone pair electrons and combine with Cd(II), which can effectively and quickly adsorb Cd(II) in aqueous solution. Thirdly, $MnFe_2O_4$ has certain oxidation ability under acidic conditions, which can increase the removal rate of Cd(II) [36].

4. Conclusions

In this study, the CTAB/$MnFe_2O_4$/MnO_2 and $MnFe_2O_4$/MnO_2 composites were successfully prepared, and their adsorption properties for Cd(II) were assessed. CTAB/$MnFe_2O_4$/MnO_2 has greater adsorption properties than $MnFe_2O_4$/MnO_2. The results indicate that the specific surface areas of CTAB/$MnFe_2O_4$/MnO_2 and $MnFe_2O_4$/MnO_2 are 166.574 and 132.947 m^2 g^{-1}, respectively. The optimum pH value for Cd(II) adsorption of the two composites is 6. The adsorption equilibrium times of CTAB/$MnFe_2O_4$/MnO_2 and $MnFe_2O_4$/MnO_2 were 270 and 400 min, respectively, according to adsorption kinetics. The adsorption process follows a pseudo-second-order kinetic model, with membrane diffusion serving as the primary rate-controlling step. Isothermal adsorption revealed that the two adsorbents could be well described by the Langmuir model. The thermodynamic parameters indicate that the adsorption process was a spontaneous, endothermic, and randomness-increasing process. The influence of coexisting ions on adsorption is primarily demonstrated in ionic strength, with cations inhibiting adsorption in the order Ca(II) > Mg(II) > Na(I). Similarly, the cadmium removal effect of organic acids increases with the increase of acid concentration, and the order of promoting effect from strong to weak is as follows: citric acid > tartaric acid > oxalic acid. Therefore, CTAB/$MnFe_2O_4$/MnO_2 is a promising and environmentally friendly adsorbent for the removal of Cd(II) from an aqueous solution.

Funding

This research was funded by National Natural Science Foundation of China (Grant No. 41807350), the Liaoning Province Education Administration (LQ2019017), and the Liaoning Province Education Administration (LQ2020008).

References

[1] A.M. Hameed, A. Alharbi, E.A. Abdelrahman, E.M. Mabrouk, R.M. Hegazey, F.K. Algethami, Y.O. Al-Ghamdi, H.M. Youssef, Facile hydrothermal fabrication of analcime and zeolite X for efficient removal of Cd(II) ions from aqueous media and polluted water, J. Inorg. Organomet. Polym. Mater., 30 (2020) 4117–4128.
[2] E.A.M. Ali, M.A. Sayed, T.M.A. Abdel-Rahman, R. Hussein, Fungal remediation of Cd(II) from wastewater using immobilization techniques, RSC Adv., 11 (2021) 4853–4863.
[3] Ihsanullah, A. Abbas, A.M. Al-Amer, T. Laoui, M.J. Al-Marri, M.S. Nasser, M. Khraisheh, M.A. Atieh, Heavy metal removal from aqueous solution by advanced carbon nanotubes: critical review of adsorption applications, Sep. Purif. Technol., 157 (2016) 141–161.
[4] K. Wang, J.W. Gu, N. Yin, Efficient removal of Pb(II) and Cd(II) using NH_2-functionalized Zr-MOFs *via* rapid microwave-promoted synthesis, Ind. Eng. Chem. Res., 56 (2017) 1880–1887.
[5] L.K. Zhang, J.Y. Guo, X.M. Huang, W.D. Wang, P. Sun, Y.M. Li, J.H. Han, Functionalized biochar-supported magnetic $MnFe_2O_4$ nanocomposite for the removal of Pb(II) and Cd(II), RSC Adv., 9 (2019) 365–376.
[6] L. Song, Y.F. Feng, C.Q. Zhu, F.Q. Liu, A.M. Li, Enhanced synergistic removal of Cr(VI) and Cd(II) with bi-functional biomass-based composites, J. Hazard. Mater., 388 (2020) 121776, doi: 10.1016/j.jhazmat.2019.121776.
[7] S.Z. Guo, K. Wu, Y. Gao, L.H. Liu, X.X. Zhu, X.L. Li, F. Zhang, Efficient removal of Zn(II), Pb(II), and Cd(II) in waste water based on magnetic graphitic carbon nitride materials with enhanced adsorption capacity, J. Chem. Eng. Data., 63 (2018) 3902–3912.
[8] A. Jusoh, L.S. Shiung, N. Ali, M. Noor, A simulation study of the removal efficiency of granular activated carbon on cadmium and lead, Desalination, 206 (2007) 9–16.
[9] Y. Wei, Z.G. Liu, X.Y. Yu, L. Wang, J.H. Liu, X.J. Huang, O_2-plasma oxidized multi-walled carbon nanotubes for Cd(II) and Pb(II) detection: evidence of adsorption capacity for electrochemical sensing, Electrochem. Commun., 13 (2011) 1506–1509.
[10] S. Kumar, R.R. Nair, P.B. Pillai, S.N. Gupta, M.A.R. Iyengar, A.K. Sood, Graphene oxide-$MnFe_2O_4$ magnetic nanohybrids for efficient removal of lead and arsenic from water, ACS Appl. Mater. Interfaces, 6 (2014) 17426–17436.
[11] N. Li, W.B. Li, F.L. Fu, Removal of chromium(VI) by $MnFe_2O_4$ and ferrous ion: synergetic effects and reaction mechanism, Environ. Sci. Pollut. Res., 26 (2019) 30498–30507.
[12] J. Liu, S.X. Ren, J.L. Cao, D.C.W. Tsang, J.Z. Beiyuan, Y.T. Peng, F. Fang, J.Y. She, M.L. Yin, N.P. Shen, J. Wang, Highly efficient removal of thallium in wastewater by $MnFe_2O_4$-biochar composite, J. Hazard. Mater., 401 (2021) 123311, doi: 10.1016/j.jhazmat.2020.123311.
[13] Q. Chen, J.W. Zheng, Q. Yang, Z. Dang, L.J. Zhang, Insights into the glyphosate adsorption behavior and mechanism by a $MnFe_2O_4$@Cellulose activated carbon magnetic hybrid, ACS Appl. Mater. Interfaces, 11 (2019) 15478–15488.
[14] S.J. Chen, F.C. Xie, Selective adsorption of copper(II) ions in mixed solution by Fe_3O_4-MnO_2-EDTA magnetic nanoparticles, Appl. Surf. Sci., 507 (2020) 145090, doi: 10.1016/j.apsusc.2019.145090.
[15] S. Harendra, C. Vipulanandan, Sorption and transport studies of cetyl trimethylammonium bromide (CTAB) and Triton X-100 in clayey soil, J. Environ. Sci., 25 (2013) 576–584.
[16] C.J. Yu, H. Li, H.Y. Ma, L.M. Zhang, Y. Li, Q. Lin, Characteristics and mechanism of Cu(II) adsorption on prepared calcium alginate/carboxymethyl cellulose@$MnFe_2O_4$, Polym. Bull., 79 (2022) 1201–1216.
[17] C.X. Zhu, Y.X. Liu, C. Huo, H.Z. Liu, Enhancing the light olefin selectivity of an iron-based fischer–tropsch synthesis catalyst by modification with CTAB, RSC Adv., 8 (2018) 32073–32083.
[18] S.H. Yao, X.L. Zhu, Y. Wang, D.N. Zhang, S.F. Wang, Y.F. Jia, Simultaneous oxidation and removal of Sb(III) from water by using synthesized CTAB/$MnFe_2O_4$/MnO_2 composite, Chemosphere, 245 (2020) 125601, doi: 10.1016/j.chemosphere.2019.125601.
[19] J.W. Lin, X.X. Wang, Y.H. Zhan, Effect of precipitation pH and coexisting magnesium ion on phosphate adsorption onto hydrous zirconium oxide, J. Environ. Sci., 76 (2019) 167–187.
[20] R. Xu, G. Zhou, Y. Tang, L. Chu, C. Liu, Z. Zeng, S. Luo, New double network hydrogel adsorbent: highly efficient removal of Cd(II) and Mn(II) ions in aqueous solution, Chem. Eng. J., 275 (2015) 179–188.
[21] S. Azizian, Kinetic models of sorption: a theoretical analysis, J. Colloid Interface Sci., 276 (2004) 47–52.
[22] Y.S. Ho, Second-order kinetic model for the sorption of cadmium onto tree fern: a comparison of linear and non-linear methods, Water Res., 40 (2006) 119–125.
[23] F.C. Wu, R.L. Tseng, R.S. Juang, Initial behavior of intraparticle diffusion model used in the description of adsorption kinetics, Chem. Eng. J., 153 (2009) 1–8.
[24] X. Guo, J.L. Wang, A general kinetic model for adsorption: theoretical analysis and modeling, J. Mol. Liq.., 288 (2019) 111100, doi: 10.1016/j.molliq.2019.111100.
[25] Y.S. Zhao, Q. Li, H.J. Ren, R. Zhou, Activation of persulfate by magnetic $MnFe_2O_4$-bentonite for catalytic degradation of 2,4-dichlorophenol in aqueous solutions, Chem. Res. Chin. Univ., 33 (2017) 415–421.
[26] Y.Y. Wang, H.Y. Ji, H.H. Lu, Y.X. Liu, R.Q. Yang, L.L. He, S.M. Yang, Simultaneous removal of Sb(III) and Cd(II) in water by adsorption onto a $MnFe_2O_4$-biochar nanocomposite, RSC Adv., 8 (2018) 3264–3273.
[27] L. Zhu, Z. Shi, L. Deng, Y. Duan, Efficient degradation of sulfadiazine using magnetically recoverable $MnFe_2O_4$/δ-MnO_2 hybrid as a heterogeneous catalyst of peroxymonosulfate, Colloids Surf., A., 609 (2021) 125637, doi: 10.1016/j.colsurfa.2020.125637.
[28] U. Lamdab, K. Wetchakun, W. Kangwansupamonkon, N. Wetchakun, Effect of a pH-controlled co-precipitation process on Rhodamine B adsorption of $MnFe_2O_4$ nanoparticles, RSC Adv., 8 (2018) 6709–6718.
[29] C.Z. Jin, G.X. Teng, Y. Gu, H. Cheng, S.P. Fu, C. Zhang, W.G. Ma, Functionalized hollow $MnFe_2O_4$ nanospheres: design, applications and mechanism for efficient adsorption of heavy metal ions, New J. Chem., 43 (2019) 5879–5889.
[30] M. He, Y. Zeng, F. Zhou, G. Kong, G. Wang, $MnFe_2O_4$ nanoparticles anchored on the surface of MgAl-layered double hydroxide nanoplates for stable magnetorheological fluids, J. Mol. Liq., 319 (2020) 114098, doi: 10.1016/j.molliq.2020.114098.
[31] K. Shoueir, H. El-Sheshtawy, M. Misbah, H. El-Hosainy, I. El-Mehasseb, M. El-Kemary, Fenton-like nanocatalyst for photodegradation of methylene blue under visible light activated by hybrid green DNSA@Chitosan@$MnFe_2O_4$, Carbohydr. Polym., 197 (2018) 17–28.
[32] B. Boutra, N. Güy, M. Özacar, M. Trari, Magnetically separable $MnFe_2O_4$/TA/ZnO nanocomposites for photocatalytic degradation of Congo red under visible light, J. Magn. Magn. Mater., 497 (2020) 165994, doi: 10.1016/j.jmmm.2019.165994.
[33] R.D.R. Kahmei, J.P. Borah, Clustering of $MnFe_2O_4$ nanoparticles and the effect of field intensity in the generation of heat for hyperthermia application, Nanotechnology, 30 (2019) 035706.
[34] S.S. Elanchezhiyan, S.M. Prabhu, J.H. Han, Y.M. Kim, Y. Yoon, C.M. Park, Synthesis and characterization of novel magnetic Zr-$MnFe_2O_4$@rGO nanohybrid for efficient removal of PFOA and PFOS from aqueous solutions, Appl. Surf. Sci., 528 (2020) 146579, doi: 10.1016/j.apsusc.2020.146579.
[35] A. Wang, Y. Chu, T. Muhmood, M.Z. Xia, Y. Xu, L. Yang, W. Lei, F.Y. Wang, Adsorption properties of Pb^{2+} by amino group's

functionalized montmorillonite from aqueous solutions, J. Chem. Eng. Data, 63 (2018) 2940–2949.
[36] N. Li, F. Fu, J. Lu, Z. Ding, B. Tang, J. Pang, Facile preparation of magnetic mesoporous $MnFe_2O_4$@SiO_2CTAB composites for Cr(VI) adsorption and reduction, Environ. Pollut., 220 (2016) 1376–1385.
[37] W. Ding, H.L. Zheng, Y.J. Sun, Z.W. Zhao, X.Y. Zheng, Y.Y. Wu, W.L. Xiao, Activation of $MnFe_2O_4$ by sulfite for fast and efficient removal of arsenic(III) at circumneutral pH: involvement of Mn(III), J. Hazard. Mater., 403 (2021) 123623, doi: 10.1016/j.jhazmat.2020.123623.
[38] Z.Y. Duan, M.Y. Song, T.G. Li, S.L. Liu, X.J. Xu, R.G. Qin, C.H. He, Y. Wang, L.G. Xu, M.J. Zhang, Characterization and adsorption properties of cross-linked yeast/β-cyclodextrin polymers for Pb(II) and Cd(II) adsorption, RSC Adv., 8 (2018) 31542–31554.
[39] J.P. Simonin, On the comparison of pseudo-first-order and pseudo-second-order rate laws in the modeling of adsorption kinetics, Chem. Eng. J., 300 (2016) 254–263.
[40] D. Kołodyńska, J. Krukowska, P. Thomas, Comparison of sorption and desorption studies of heavy metal ions from biochar and commercial active carbon, Chem. Eng. J., 307 (2017) 353–363.
[41] N.A. Oladoja, A.K. Akinlab, Congo red biosorption on palm kernel seed coat, Ind. Eng. Chem. Res., 48 (2009) 6188–6196.
[42] G.E. Boyd, J. Schubert, A.W. Adamson, The exchange adsorption of ions from aqueous solutions by organic zeolites. II. Kinetics, J. Am. Chem. Soc., 69 (1947) 2818–2829.
[43] Y.C. Wong, Y.S. Szeto, W.H. Cheung, G. McKay, Adsorption of acid dyes on chitosan—equilibrium isotherm analyses, Process Biochem., 39 (2004) 695–704.
[44] Y.M. Hao, M. Chen, Z.B. Hu, Effective removal of Cu(II) ions from aqueous solution by amino-functionalized magnetic nanoparticles, J. Hazard. Mater., 184 (2010) 392–399.
[45] A. Kumar, S. Prasad, P.N. Saxena, N.G. Ansari, D.K. Patel, Synthesis of an Alginate-Based Fe_3O_4–MnO_2 xerogel and its application for the concurrent elimination of Cr(VI) and Cd(II) from aqueous solution, ACS Omega, 6 (2021) 3931–3945.
[46] P.L. Wang, T.T. Shen, X.Y. Li, Y.Y. Tang, Y.J. Li, Magnetic mesoporous calcium carbonate-based nanocomposites for the removal of toxic Pb(II) and Cd(II) ions from water, ACS Appl. Nano Mater., 3 (2020) 1272–1281.
[47] W.Q. Zuo, C. Chen, H.J. Cui, M.L. Fu, Enhanced removal of Cd(II) from aqueous solution using $CaCO_3$ nanoparticle modified sewage sludge biochar, RSC Adv., 7 (2017) 16238–16243.
[48] J. Liang, X.M. Li, Z.G. Yu, G.M. Zeng, Y. Luo, L.B. Jiang, Z.X. Yang, Y.Y. Qian, H.P. Wu, Amorphous MnO_2 modified biochar derived from aerobically composted swine manure for adsorption of Pb(II) and Cd(II), ACS Sustainable Chem. Eng., 5 (2017) 5049–5058.
[49] Y. Xian, J. Wu, G. Yang, R.T. Liao, X.H. Zhang, H. Peng, X.Y. Yu, F. Shen, L. Li, L.L. Wang, Adsorption characteristics of Cd(II) in aqueous solutions using spent mushroom substrate biochars produced at different pyrolysis temperatures, RSC Adv., 8 (2018) 28002–28012.
[50] K. Attar, D. Bouazza, H. Miloudi, A. Tayeb, A. Boos, A.M. Sastre, H. Demey, Cadmium removal by a low-cost magadiite-based material: characterization and sorption applications, J. Environ. Chem. Eng., 6 (2018) 5351–5360.
[51] J.J. Zhao, Y.Z. Niu, B. Ren, H. Chen, S.X. Zhang, J. Jin, Y. Zhang, Synthesis of Schiff base functionalized superparamagnetic Fe_3O_4 composites for effective removal of Pb(II) and Cd(II) from aqueous solution, Chem. Eng. J., 347 (2018) 574–584.
[52] A.K. Fard, G. Mckay, Y. Manawi, Z. Malaibari, M.A. Hussien, Outstanding adsorption performance of high aspect ratio and super-hydrophobic carbon nanotubes for oil removal, Chemosphere, 164 (2016) 142–155.
[53] G.R.D. Freitas, M.G.A. Vieira, M.G.C.D. Silva, Batch and fixed bed biosorption of copper by acidified algae waste biomass, Ind. Eng. Chem. Res., 57 (2018) 11767–11777.
[54] A. Ajmal, P.R. Piergioyanni, Effect of mordanting on the adsorption thermodynamics and kinetics of cochineal for wool, Ind. Eng. Chem. Res., 57 (2018) 4462–4469.
[55] C. Wu, X.F. Lou, X.F. Xu, A.M. Huang, M. Zhang, L. Ma, Thermodynamics and kinetics of pretilachlor adsorption on organobentonites for controlled release, ACS Omega, 5 (2020) 4191–4199.
[56] X. Chen, X. Jiang, C.J. Yin, B.L. Zhang, Q.Y. Zhang, Facile fabrication of hierarchical porous ZIF-8 for enhanced adsorption of antibiotics, J. Hazard. Mater., 367 (2019) 194–204.
[57] H.X. Zhu, X.J. Cao, Y.C. He, Q.J. Kong, H. He, J. Wang, Removal of Cu^{2+} from aqueous solutions by the novel modified bagasse pulp cellulose: kinetics, isotherm and mechanism, Carbohydr. Polym., 129 (2015) 115–126.
[58] Q.B. Kong, B.B. Xie, S. Preis, Y. Hu, H.Z. Wu, C.H. Wei, Adsorption of Cd^{2+} by an ion-imprinted thiol-functionalized polymer in competition with heavy metal ions and organic acids, RSC Adv., 8 (2018) 8950–8960.